Hindawi
Advances in Materials Science and Engineering
Volume 2018, Article ID 1294205, 13 pages
https://doi.org/10.1155/2018/1294205

Research Article

Lightweight Photovoltaic Composite Structure on Stratospheric Airships

Xinyun Zhang,[1] Kangwen Sun ,[1] Dongdong Xu,[1] and Shijun Guo[2]

[1]*School of Aeronautic Science and Engineering, Beihang University, Beijing 100191, China*
[2]*School of Aerospace, Transport and Manufacturing, Cranfield University, Bedford MK43 0AL, UK*

Correspondence should be addressed to Kangwen Sun; sunkw100@buaa.edu.cn

Received 6 April 2018; Revised 12 September 2018; Accepted 6 November 2018; Published 10 December 2018

Academic Editor: Fabrizio Sarasini

A semirigid solar array is an efficient energy system on the surface of stratospheric airships for utilizing the solar energy, which we believe that it has succeeded in providing some impressive results for conceptual design. This paper developed a lightweight photovoltaic composite structure (LPCS) according to the characteristics of the stratospheric airship capsule. In order to improve the flexibility of the solar cell, we studied the mechanical properties in the different thicknesses of the honeycomb core for LPCS by FEM software and three-point bending test, and we also launched experiments to measure the temperature difference between upper and lower surfaces of the LPCS test samples under different solar radiation flux conditions. The experimental data were examined to evaluate the mechanical properties and thermal insulation performances of LPCS. Considering the quality of the whole structure, the paper finally comes up with the conclusion of the optimal thickness of the honeycomb core with further detailed descriptions.

1. Introduction

As a high-altitude platform, stratospheric airships are widely concerned in many important fields, especially in communication, broadcasting, remote sensing, scientific research, and so forth. Currently, United States, Japan, and South Korea are the major countries to develop stratospheric airships [1–10].

Solar energy is an ideal choice to provide power for high-altitude and long-endurance airships. This type of power system is actually a photovoltaic (PV) array coupled to an energy storage system [11]. At present, monocrystalline silicon solar cells and polycrystalline silicon and amorphous silicon thin-film solar cells are mainly used in solar battery applications. Among all the solar cells, monocrystalline silicon solar cell is the most technically matured and widely used. However, still some shortcomings exist such as hard rigidity and poor toughness for mono-Si to be applied in the surface capsule. At the same time, large-scale production of amorphous silicon solar cells and amorphous silicon thin-film solar cells is limited to apply to the stratosphere airship because of the rather low photoelectric conversion efficiency and "optical-induced degradation" [12]. This research aimed at studying a flexible processing of monocrystalline silicon solar cell (mono-Si solar cell) that can be applied to stratospheric airships under low ambient temperature and high solar irradiation flux conditions. On the one hand, the rarefied air and low ambient temperature in the stratosphere would lead to low convective heat conduction and high solar radiation flux, which make the temperature in the stratosphere prone to be overheating or undercooling [11, 13]. In particular, as shown in Figure 1, the solar cell array with high solar absorptivity may serve as the high-temperature heat source at noon and heat the envelope and inner lift gas of the airship [14]. The simulation results indicated that since the solar cells have high solar absorptivity, the maximum temperature on the PV panel would reach about 370 K at noon, which is above the highest temperature of the envelope without the PV panel (320 K) during the summer solstice and even aggravated the overheating problem. In the photovoltaic installed area, the largest temperature difference between PV panel and envelope could also reach 33 K. On the other hand, the solar cell array has a certain amount of flexibility, and they bend but do not break on the airship

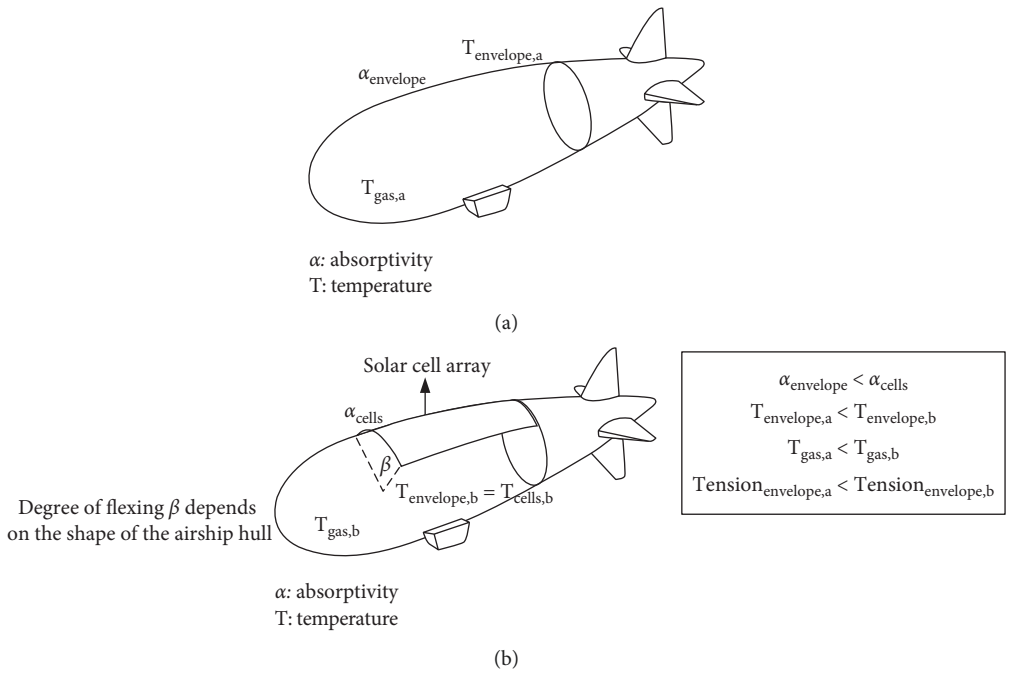

Figure 1: Schematic diagram of the airship (a) without and (b) with solar array.

hull like other brittle materials do. The popularity of stratospheric airships brings increasing demands for several key technologies of these long-duration lighter-than-air vehicles [15, 16]. The solar array is one of the key technologies among these demands because the vehicles require the ability of long-duration fly at high altitudes, especially the flexible processing of the monocrystalline silicon solar cell that is designed in thermal protection systems to keep the temperature of underlying structure within an acceptable range.

According to the characteristics of the stratospheric airship capsule and mono-Si solar cell, this paper develops a lightweight photovoltaic composite structure (LPCS), in which the mono-Si solar cell of modified PET packaged as the surface to the asymmetric honeycomb core. A glass-fiber ribbon was used to improve the stiffness characteristic of the structure. The comparison results with experimental data and the theoretical model show that LPCS can not only solve overheating problems on the lower surface of a solar cell for stratospheric airships but also improve the overall flexibility of the mono-Si solar cell and reduce the stress concentration effectively.

Based on the current search, the thermal insulation requirements of solar effects have an effect not only on the solar cell efficiency but also on the thermodynamic characteristics of an airship [17, 18]. LPCS on the stratospheric airship is designed to study the mechanical properties and thermal insulation properties in this paper. The experiments of LPCS with different thicknesses of honeycomb by three-point bending have been conducted, and an experiment to measure temperature difference between upper and lower surfaces of LPCS under different solar radiation flux conditions has been designed. The FE models of LPCS with different thicknesses of honeycomb are built up, and then numerical simulation was implemented by using the software ABAQUS. Considering the quality of the whole structure, the article finally gives the conclusion of the optimal thickness of the honeycomb core with more detailed descriptions.

2. Physical Model

By determining the encapsulation materials, high-strength fiber material and low-density flexible insulation material, and combining with the characteristics of the stratospheric airship envelope, an implement method for engineering application systems for a lightweight photovoltaic composite structure (LPCS) is described.

2.1. Typical Selection of Composite Structure. Based on existing flexible insulation structures and enhancement structures, we develop an LPCS by virtue of modified PET (polyethylene terephthalate), 22% efficiency of mono-Si solar cells, fiberglass mesh, epoxy resin film or EVA (ethylene-vinyl acetate copolymer) film, and Nomex honeycomb. The solar cells with membrane surface encapsulation by EVA and modified PET film were used, in order to better stiffness matching with honeycomb core layer. The fiberglass has high mechanical strength and can be used as the enhancement structure. The epoxy resin or EVA film can be used as adhesive to combine each layer together. The Nomex honeycomb can effectively reduce the stress concentration of the overall structure, improve the structure's load-bearing characteristics, and also has a great capability of thermal insulation. The LPCS connects the stratospheric airship envelope through the mechanical fastening way. The structure is shown in Figure 2.

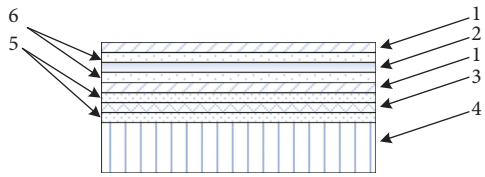

Figure 2: The multilayer composite structure of the solar cells. *Note.* 1: modified PET; 2: silicon solar cell; 3: fiberglass mesh; 4: Nomex honeycomb paper; 5: epoxy resin; 6: EVA.

3. Static Comparative Tests

The static comparative test aims to provide reliable mechanical performance parameters for analysis and optimization of LPCS, and the reliability of the asymmetric honeycomb sandwich structure (AHSS) was validated preliminarily All tests were conducted in the WDS-500 machine at a constant velocity of 5 mm/min as shown in Figure 3. The dimensions of the mono-Si solar cell specimens were 125 mm (length) × 125 mm (width) × 0.29 mm (thickness). The dimensions after EVA encapsulation were 125 mm (length) × 125 mm (width) × 0.49 mm (thickness). The dimensions of 2 mm honeycomb-laminated specimens were 125 mm (length) × 125 mm (width) × 2.74 mm (thickness). The specimens were placed on two supporting rollers with a span of 90 mm.

As the LPCS underwent high deformation during the bending test, simple linear beam theory was not sufficient to calculate the stress on the cells [19]. A model was used to take the large deflections into account.

3.1. A Model for Calculating the Large Deformation under Three-Point Bending Test. As the LPCS underwent high deformation during the bending test, simple linear beam theory was not sufficient to calculate the stress on the cells. A model similar to the one developed by Schoenfelder et al. [20] was used to take the large deflections into account.

With the classic linear beam theory, the maximum moment in the center of the cell is

$$M_{\max} = \frac{PL}{4}, \tag{1}$$

where P is the load applied and L is the span. The maximum stress at the surface of the cell is then

$$\sigma_{\max} = \frac{M_{\max}}{I}\frac{t}{2} = \frac{6M_{\max}}{Bt^2}, \tag{2}$$

where I is the moment of inertia of the cell in flexion, B is the width, and t is the thickness of the cell.

When the deformations are larger, the orientation of the reaction forces, the effective span, and the effective displacement change. Figure 4 illustrates the difference between small displacements approximation and large displacements model.

The reaction force becomes

$$F = \frac{P}{2\cos(\theta)}. \tag{3}$$

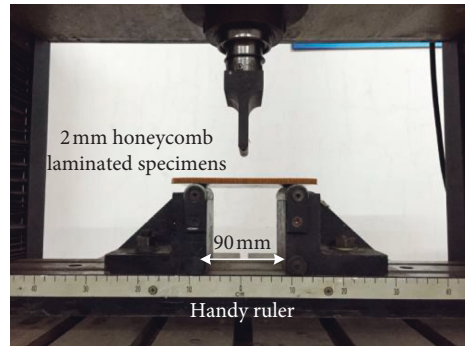

Figure 3: Three-point bending test of the laminated solar cells.

In order to approximate the angle θ, the deformed shape of the cell is assumed to follow linear beam theory and is expressed as

$$y(x) = \frac{4\delta}{L_2^3}\left(\frac{3L_2}{2}x^2 - x^3\right), \tag{4}$$

where x is the span in the Cartesian coordinates and δ is the deflection at the center so $x = L_2/2$. The angle θ is then defined by

$$\tan(\theta) = \dot{y}\left(\frac{L_2}{2}\right) = \frac{3\delta}{L_2}. \tag{5}$$

The moment under the loading point can then be calculated as

$$M_{\max} = \frac{PL_n}{4} + F\sin(\theta)\delta_n = \frac{PL_n}{4} + \frac{3P\delta_n^2}{2L_n}. \tag{6}$$

With $L_n = L_2 - 2r\sin(\theta)$, $\delta_n = \delta - r(1-\cos(\theta))$.

If the friction on the supporting pins is disregarded, the maximum stress can then be calculated with equation (1).

3.2. The Comparison of Test and Analysis. As solar cells are very brittle, brittle fracture occurs when the crack expands to critical size. The LPCS was fabricated with one solar cell as face, so we tested the solar cell in three-point bending. All the solar cells broke at a 45° angle to the loading direction, as observed on the broken sample in Figure 5. This is explained by two reasons. Firstly, this is the maximum shear direction, and secondly, in the mono-Si solar cell as a kind of brittle materials, the angle of transverse bending normal stress and shear stress near the upper roller is about 90° and the resultant force direction is about 45°. Therefore, the mono-Si solar cell is the relatively weaker orthotropic materials, so we take it as orthogonal isotropic material to simplify calculations. But in order to reduce errors of the contrast test, all the main gate line of specimens are placed in parallel with the upper roller.

All materials used in the array fabrication, modified PET, solar cells, and EVA, are isotropic, so the mechanical property of the mono-Si solar cell after encapsulated by modified PET is isotropic as a whole. Previous experimental data and theory have proven that a honeycomb core can be classified as an orthotropic material based on the hexagonal

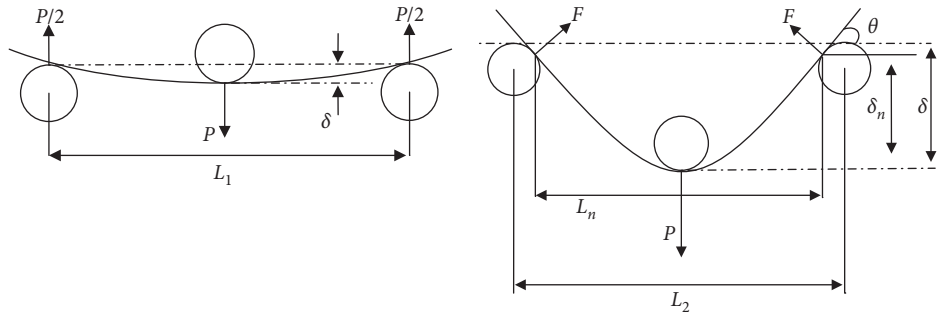

Figure 4: Large and small deformations of the three-point bending test.

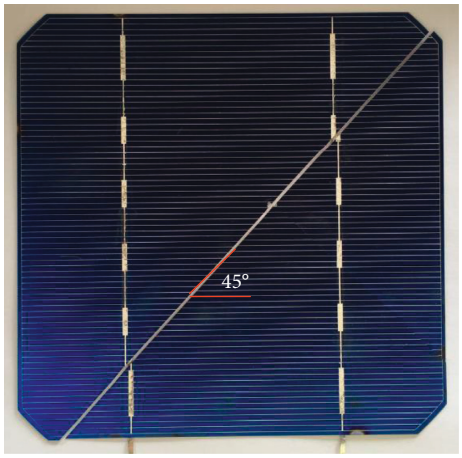

Figure 5: The fracture photograph of the solar cell after the three-point bending test.

grid of honeycomb cellular [21]. So, the whole mechanical property of LPCS is orthotropic as shown in Figure 6.

The mono-Si solar cell is not brittle after encapsulation by modified PET, and the fracture position is hard to find. Through encapsulating and laminating, pressure can spread by EVA and honeycomb core layer to nonstressed location, preventing local buckling and microcracks from appearing on the edge of the mono-Si solar cell and reducing stress concentration. At the same time, the toughness of EVA also prevents cracks from propagating.

According to the results of the test (Table 1), after encapsulated and laminated by modified PET, the maximum equivalent bending stress of the mono-Si solar cell decreased, while the maximum bending strain increased. The equivalent bending elastic modulus is only 2.41% after encapsulation and the deflection increased by 38.03%. The flexibility of the solar cell is effectively improved, which can enhance the ability to resist damage to a certain extent.

4. Simulation of Multilayer Composite Structure

According to the sealing property of LPCS, stress and strain of mono-Si solar cell cannot be measured. As each layer of LPCS has different material strength and thickness, the test cannot determine if there is a fragile failure under the condition of three-point bending. So in this paper, a last-ply failure (LPF) analysis method for LPCS is incorporated in the finite element code in ABAQUS/CAE with test specification.

4.1. Finite Element Analysis Model. Finite element software package ABAQUS/standard is used for the finite element modeling and simulation of the LPCS in different thicknesses like 2 mm, 5 mm, and 8 mm. The geometrical model, contact property, boundary condition, and load step are modeled and settled in ABAQUS/CAE, and the mechanical properties of modified PET, EVA, and others are given and listed in Table 2 [22–24]. A user-defined material subroutine (UMAT) is developed to introduce the strength analysis method mentioned above into the simulation.

The meshing scheme of the model is shown in Figure 7. An eight-node reduced integration element with hourglass control (C3D8R) and a four-node bilinear rigid quadrilateral element (R3D4) are implemented for mesh discretization of the 3D braided composite specimen and rollers.

4.2. Equivalent Mechanical Performance of Honeycomb Core Layer. Based on the LPCS model, with a view to the discrete heterogeneity of the honeycomb material, to simplify the analysis, the honeycomb core area is simulated to the orthogonal anisotropic body equivalent unit. This places a lot of emphasis on the selection of the equivalent model.

4.3. Equivalent Calculation of Elastic Moduli E_1 and E_2. For loading in the X and Y directions as shown in Figure 8, the depth of the honeycomb cell is b. By the symmetry of the honeycomb cell, single layer thickness of the hole wall is analyzed, and it has length l. By the condition of equilibrium, $F = 0$, $W = \sigma_1 lb \sin(\theta)$, so

$$M = \frac{Wl \sin(\theta)}{2}. \tag{7}$$

The wall deflects by

$$\delta = \frac{Wl^3 \sin\theta}{12E_s I}. \tag{8}$$

Of this, a component β is parallel to the X-axis, giving a strain

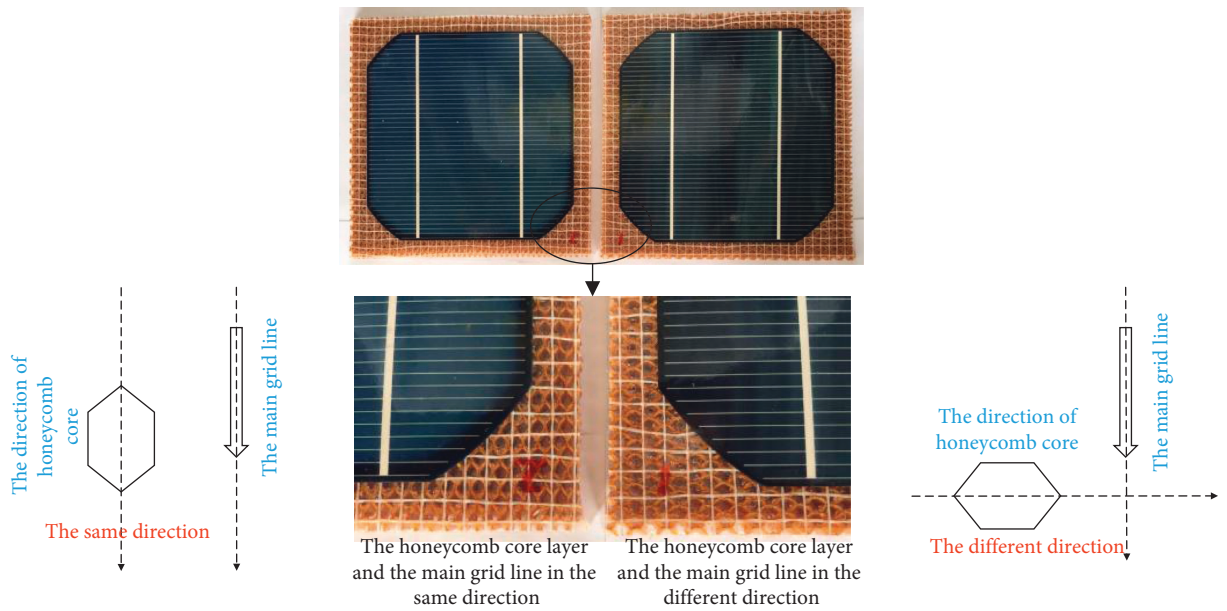

Figure 6: The contrast test for different laminated directions of the honeycomb core layer.

Table 1: The results of the three-point bending test for solar cells.

The types of the solar cell	The maximum equivalent bending stress (MPa)	Maximum strain (%)	Deflection (mm)	The equivalent elastic modulus (GPa)
EVA encapsulation	27.45	0.79	6.1	3.48
Different directions of the honeycomb core	1.35	1.33	6.52	0.101
The same direction of the honeycomb core	1.22	1.46	8.42	0.084

Table 2: The mechanical properties.

The type of mechanical properties	Modified PET	EVA	The solar cell	Fiberglass mesh	Epoxy resin film
E (GPa)	0.837	0.655	52.12	11.4	1.1
Poisson's ratio (μ)	0.42	0.3	0.3	0.28	0.38
Thickness (mm)	0.05	0.2	0.29	0.14	0.2

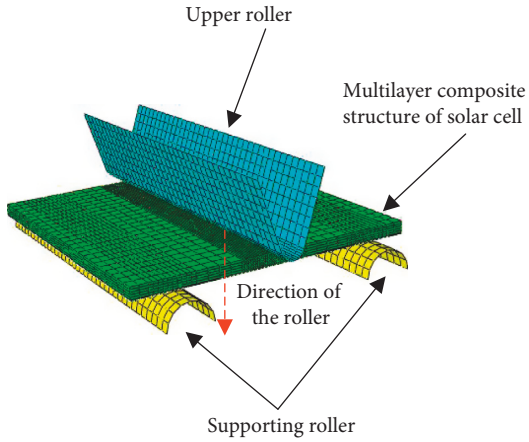

Figure 7: The finite element mesh model of the bending test about multilayer composite structure of solar cells.

$$\varepsilon_1 = \frac{\delta \sin\theta}{a + l\cos\theta} = \frac{\sigma_1 l^4 \sin^3\theta}{t^3 E_s (a + l\cos\theta)}. \quad (9)$$

From which, Young's modulus parallel to the X-axis is $E_1 = \sigma_1/\varepsilon_1$, so

$$E_1 = E_s\left(\frac{t}{l}\right)^3 \frac{a/l + \cos\theta}{\sin^3\theta}. \quad (10)$$

Similarly, Young's modulus parallel to the Y-axis is $E_2 = \sigma_2/\varepsilon_2$, so

$$E_2 = E_s\left(\frac{t}{l}\right)^3 \frac{\sin\theta}{(a/l + \cos\theta)\cos^2\theta}. \quad (11)$$

4.4. Calculation of Shear Modulus G_1. The calculation of the shear modulus is illustrated in Figure 9. The improvement of the model hypotheses is emphasized during the modeling:

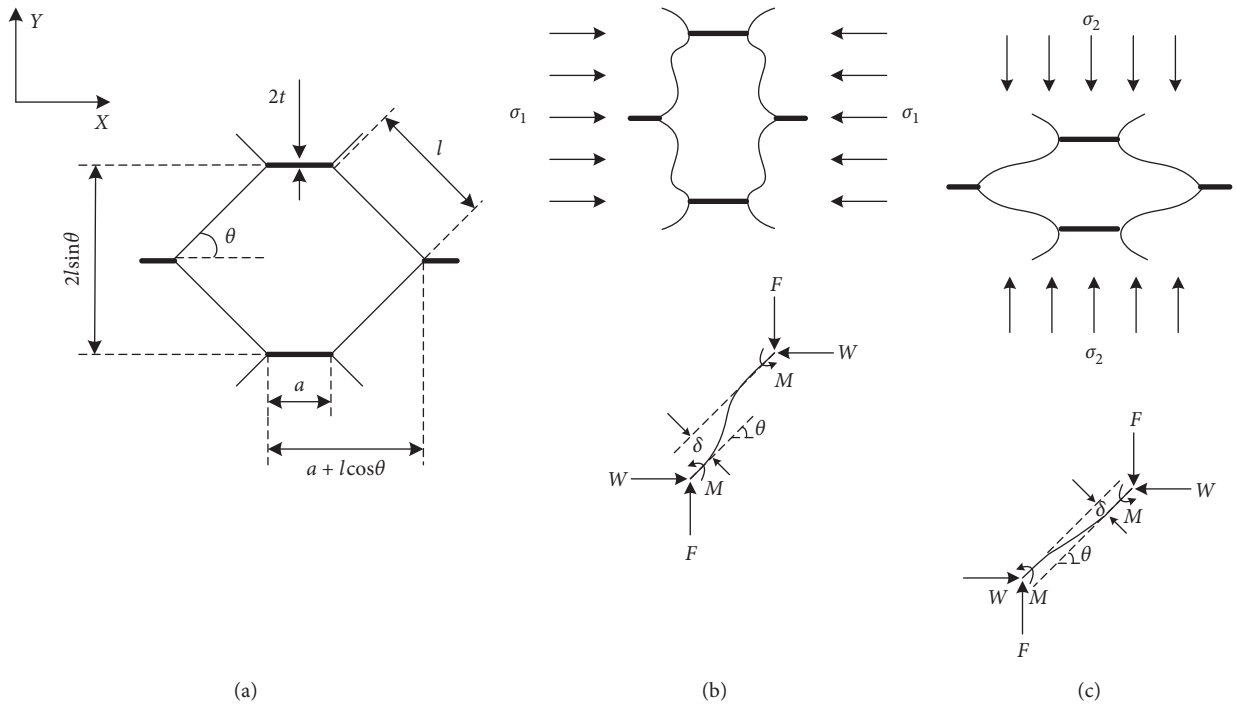

Figure 8: (a) Unloaded. (b) Bending load in the X direction. (c) Bending load in the Y direction.

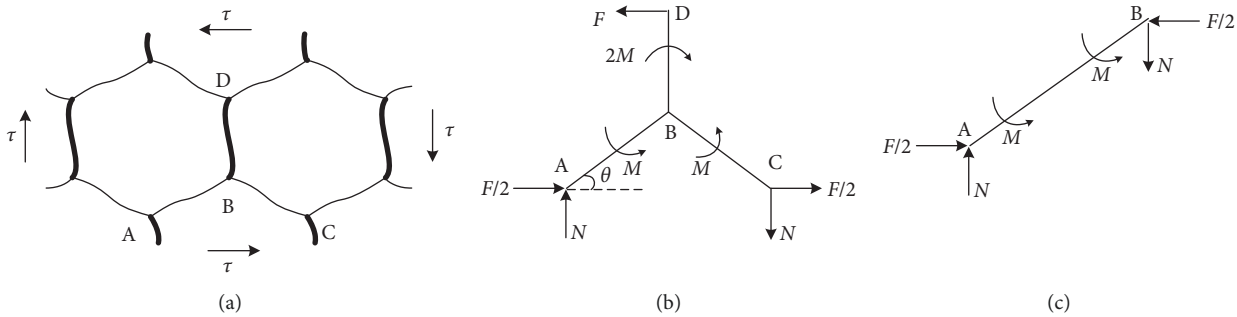

Figure 9: Cell deformation under shear stress.

(1) By symmetry, there is no relative motion of the points A, B, and C

(2) Assume that each node is around the same angle

(3) The shearing deflection of the structure is entirely due to the bending of beam BD and its rotation about the point B

The forces are shown in Figure 9. By summing moments at B, we find the moment applied to the members AB and BC is $M = Fa/4$.

All the joints rotate through an angle φ. Then, since there is no deflection of B with respect to A, we have

$$\varphi = \frac{M_A l}{3E_s I_1} - \frac{M_B l}{6E_s I_1} = \frac{Fal}{24E_s I_1}. \tag{12}$$

Assume that shear deformation consists of the rotation of the cell wall BD around point B and bending formation of BD. So $\mu_{BD} = \varphi a + \delta_{BD}$, and

$$\delta_{BD} = F\frac{a^3}{3EI_2} - 2M\frac{a^2}{2EI_2}. \tag{13}$$

The value for μ_{BD} is as follows:

$$\mu_{BD} = \frac{Fa^3}{12EI_2} + \frac{Fa^2 l}{24EI_1} = \frac{Fa^2}{24EI_1}\left(\frac{a}{4} + l\right). \tag{14}$$

The shear strain

$$\gamma_{xy} = \frac{\mu_{BD}}{a + l\sin\theta}. \tag{15}$$

The shear stress

$$\tau = \frac{F}{2bl\cos\theta}. \tag{16}$$

So, the shear modulus G_1 is given as follows:

$$G_1 = \frac{\tau}{\gamma_{xy}} = E_s\left(\frac{t}{l}\right)^3 \frac{(a/l + \sin\theta)}{(a/l)^2\cos\theta(a/4l + 1)}. \tag{17}$$

Table 3: The equivalent mechanical properties of honeycomb.

Type	Values
Double hole wall, a	1.5 mm
Honeycomb angle, θ	55°
Elastic modulus of Nomex paperboard, E_s	1780 MPa
Elastic modulus of honeycomb core layer, E_1	1.18 MPa
Shear modulus of honeycomb core layer, G_1	2.01 MPa
Single hole wall, l	2 mm
Nomex paperboard thickness, t	0.13 mm
Shear modulus of Nomex paperboard, G_s	623 MPa
Elastic modulus of honeycomb core layer, E_2	0.92 MPa

Based on the above theory, considering the actual size of the honeycomb core layer after encapsulation by modified PET, the equivalent mechanical properties of the honeycomb model was established as shown in Table 3.

5. Mechanics Performance Optimization of Multilayer Composite Structure

The comparison of the predicted load-deflection curves of the honeycomb core layer in LPCS with different thicknesses under three-point bending with that of experimental data are given in Figure 10.

5.1. Different Thicknesses of Honeycomb Core Layer Effects on Bending Properties. It is observed from Figure 10 that the load-deflection curves show a similar changing tendency of the applied load and can be divided into three stages: the initial linear elastic stage, the nonlinear stage with the minor damage evolution, and the curve descending stage with a sudden drop of the load. The linear stage exhibited the linear elastic relationship between the load and deflection and no damages occurred in the specimens. The initial damages started on the mono-Si solar cell, but multilayer structure disperses pressure and reduces stress concentration, to prevent the crack extension, and meanwhile, the load might still have a corresponding increase. The sharp drop of the load was caused by the damages occurred on the mono-Si solar cell, as shown in Figure 11. Subsequently the multilayer composite structure lost its loading capacity.

Through the comparison between the different thicknesses of the honeycomb core layer, the load-deflection curves of the initial slope and ultimate load increases with the decrease of thickness of honeycomb core layer are shown in Figure 12. But according to the asymmetry of the structure and the local buckling of the honeycomb core layer under large deformation, the nonlinear relation of load-dependent deformation occurs [25, 26].

The predicted load-deflection curves of the 2 mm, 5 mm, and 8 mm LPCS specimens under three-point bending in comparison with the experimental results are given in Figure 12. The maximum loads of the 2 mm, 5 mm, and 8 mm LPCS specimens in the experimental results are 7.11 N, 10.11 N, and 11.96 N, whereas those of the numerical predictions are 7.03 N, 9.46 N, and 11.04 N. It can be seen that good agreements are obtained in both linear and nonlinear stages between numerical prediction and experimental results. The calculation errors of the predicted maximum loads are within an acceptable range as show in Table 4.

6. Different Thicknesses of Honeycomb Core Layer Effects on Thermal-Barrier Performance

6.1. Experimental Approach. A series of experiments were conducted to optimize the thermal performance and mechanical properties of LPCS and to provide optimized models based on the thermal insulation and mechanical properties. The following is a brief description of the LPCS test sample, experimental apparatus and instrumentation, and the experimental procedure.

6.2. LPCS Test Samples. The insulation layer of the LPCS test samples is mainly composed of honeycomb core. For the present study, three kinds of the LPCS samples with different honeycomb core thicknesses were tested and compared with monocrystalline silicon solar cells. As shown in Figure 11, the thickness of honeycomb core layers for these three different types of the LPCS samples were 2 mm, 5 mm, and 8 mm, respectively. The planar size of the sample is 125 × 125 mm. The density of lightweight Nomex honeycomb is 29 kg/m^3 [27]. The solar cells studied in this experiment are monocrystalline silicon solar cells. The basic parameters of the solar cells are shown in Table 2.

6.3. Experimental Apparatus. All experimental tests were conducted in the integrated environmental test cabin, and experimental data can be obtained from related data acquisition equipment. A multiparameter large-scale environment simulation test cabin can simulate multiple parameters of the stratosphere, including items such as solar radiation heat flux, airflow velocity, cold temperature, and lower gas pressure. The test cabin is about 1.5 meters in diameter and 3.2 meters long. A heat shield cooled by liquid nitrogen surrounds the inner wall of the cabin and serves as a radiator for the test sample. The experimental apparatus for measuring the thermal performance consists of an environmental cabin, a vacuum gauge, a wet-type gas meter, a heat flow meter, a data logger, an induced draught fan, a personal computer, and a pressure gauge. As shown in Figure 13, the entire experimental apparatus and LPCS test samples were assembled in a clean room to prevent other factors.

In the course of the experiment, refer experimental design methods of Li et al. [14], the temperature and pressure in the environmental test cabin are set to the stratospheric parameters, such as the environmental temperature is 216 K and the environmental pressure is 3 kPa. The solar radiation simulated by the solar simulator irradiates the upper surfaces of the test sample in the flux range of 300–1260 W/m^2. A schematic diagram of temperature measurement points and test circuit of the whole experiment is shown in Figure 14. Figure 14 is reproduced from the study of Li et al., under the Creative Commons Attribution License/public domain. The thermocouples are fixed on both

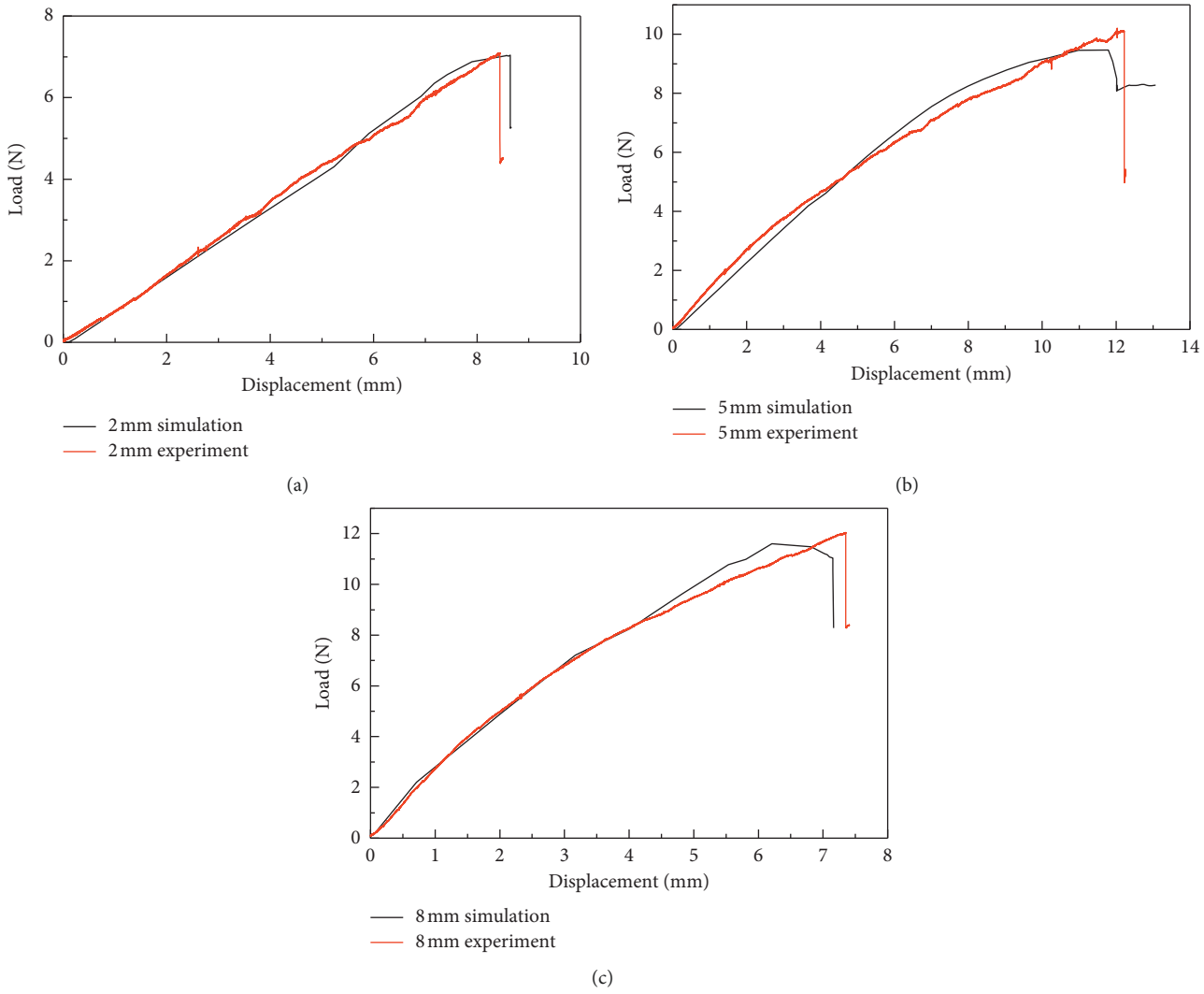

Figure 10: The load-displacement cure of the multilayer composite structure about solar cells.

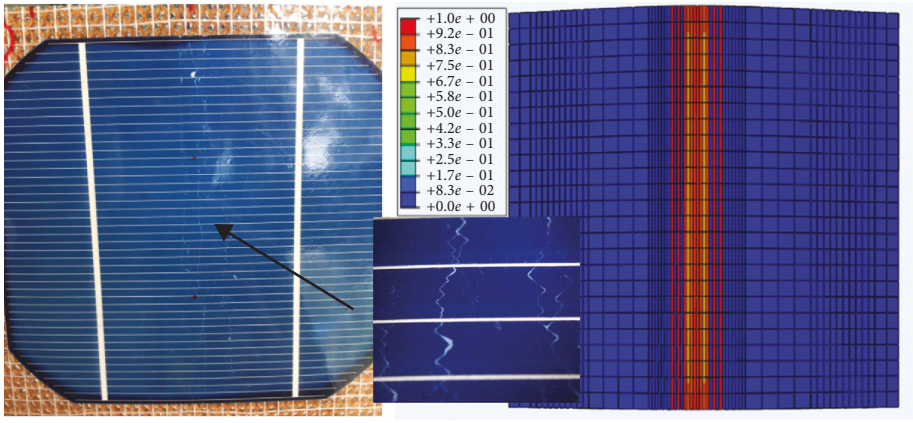

Figure 11: Damage distribution of the honeycomb core specimen with 5 mm thickness.

upper and lower surfaces in order to install on the specimen's heating surface. The thermocouple 1 is located at the middle portion of the upper surface, and the thermocouple 2 is located at the corresponding position of the lower surface. The thermocouples measure the temperatures of the upper and lower surfaces of the test samples. The temperature data are recorded by the data logger when the temperature change per 10 minutes is less than 1°.

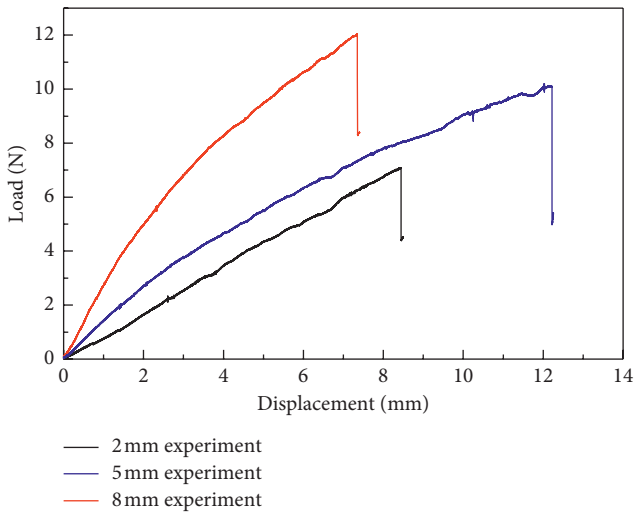

Figure 12: The result comparison about the load-displacement of the honeycomb core in different thicknesses.

Table 4: The comparison between numerical simulation results and test results.

Thickness of the honeycomb (mm)	Bending ultimate load (N)		
	Experiment	Simulation	Calculation error (%)
2	7.11	7.03	1.13
5	10.11	9.46	6.43
8	11.96	11.04	7.69

7. Results and Discussion

The experimental data of temperature difference between upper and lower surfaces at three types of LPCS and mono-Si solar cell for studying thermal performance are presented in Figure 15. The optimum design of the thermal performance is discussed. From the upper and lower surfaces of experimental date analysis and comparison, the effects of the thickness of the honeycomb core layer on the specific temperature difference are analyzed.

7.1. Experimental Results of Thermal-Barrier Performance. Based on the experimental approach in Section 6.3, some measurement results are obtained to investigate thermal insulation performance of the LPCSs. The upper and lower surface temperatures were not recorded until the temperature reached the steady state, and the results were not continuous by choosing the value of four typical irradiation. The steady-state temperature of the test samples under different irradiation conditions is shown in Figure 15. The experimental results show that the relationship between the temperature and the solar radiation flux irradiating on the sample exhibited a nonlinear relationship and has a special change trend.

The experimental results of the effects of the honeycomb core thickness on specific temperature differences are shown in Figure 16. It shows the representative results of the measurements, and the ordinate shows the specific temperature difference among three types of LPCSs and mono-Si solar cells. It is observed that there is a positive correlation between the particular temperature differences for three types of LPCSs and mono-Si solar cell, and the solar radiation flux increases. The specific temperature difference also increases with the increase of thickness under the same solar radiation. It is notable that, under the same illumination intensity, the specific temperature difference of the 8 mm test sample is the largest, and the temperature difference of monocrystalline silicon solar cells test sample is the lowest. It

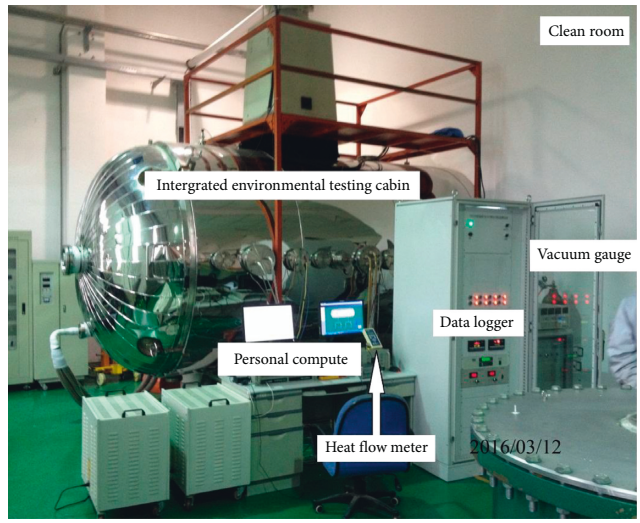

Figure 13: Photograph of the experimental apparatus.

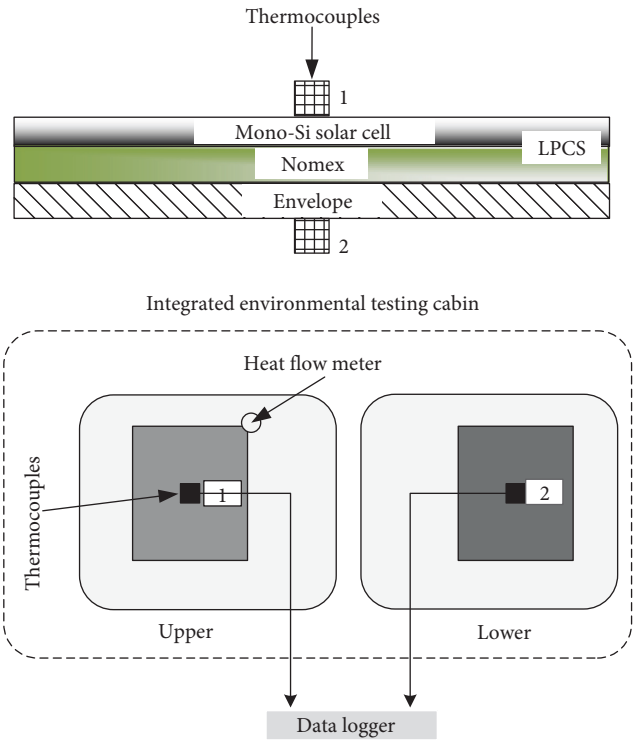

Figure 14: Schematic diagram of the temperature measurement points and test circuit (not to scale) (the figure is reproduced from the study of Li et al., under the Creative Commons Attribution License/public domain).

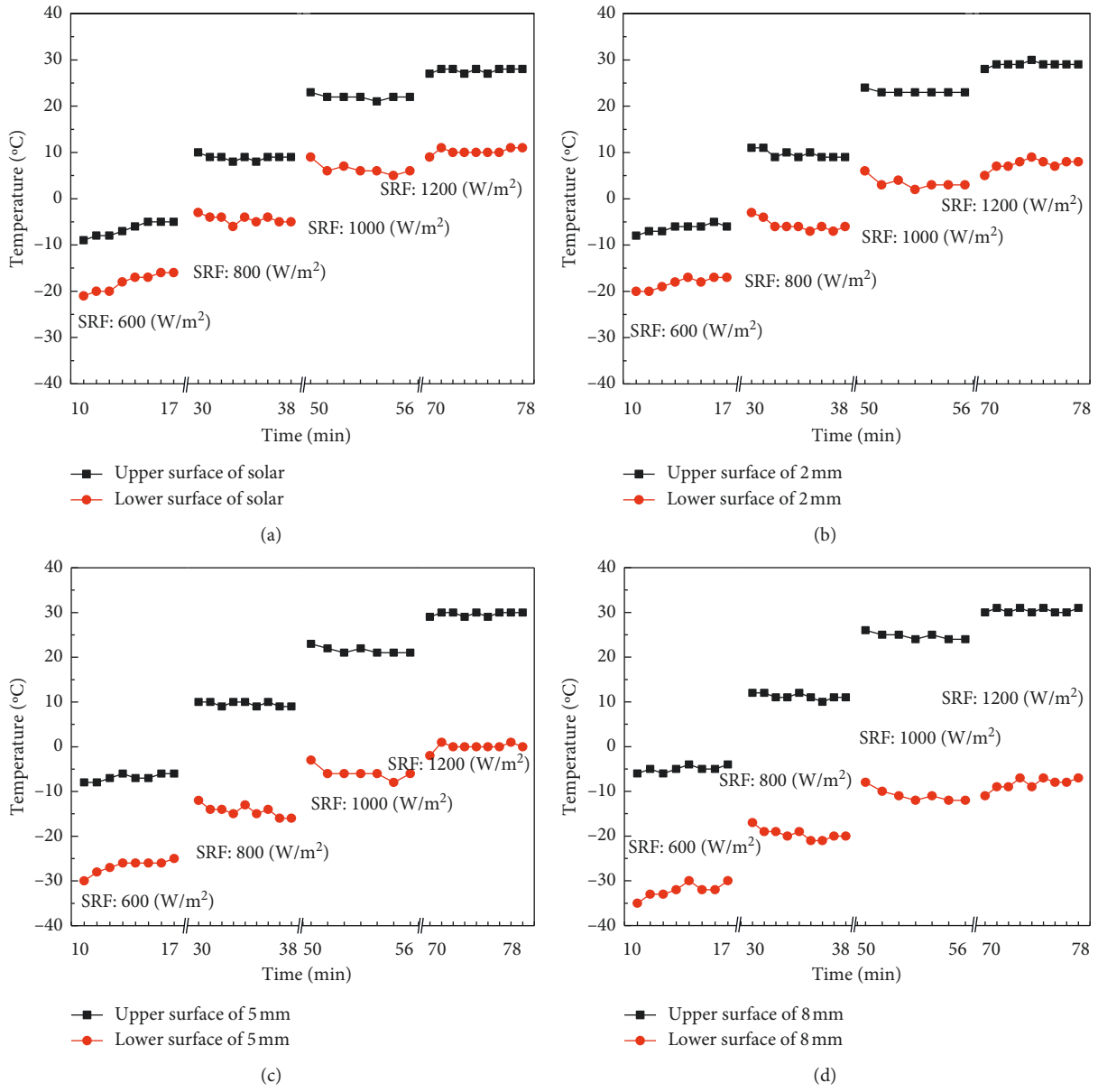

Figure 15: Test temperature data of the honeycomb core in different thicknesses (SRF: solar radiation flux).

is also important to note that this result is different from the conclusion shown in Figure 10. An optimized LPCS can be designed by combing the effect of thickness on specific temperature difference and mechanics performance.

7.2. Discussion of LPCS. This paper describes the concept of deflection weight ratio, which is used to analyze different thicknesses of the honeycomb core layer to improve the deflection of LPCS, considering the structure weight as shown in Table 5. Finally, a factor defined as the ratio of the increase of deflection to discontinuity density is used to estimate the optimal design of LPCS.

On the premise of having the same structural weight, the larger the deflection weight ratio of the LPCS, the more the effect of structure flexibility. We can see from Table 5 that, to improve the deflection of structure, 5 mm honeycomb core layer is the optimal choice compared with 2 mm and 8 mm.

Considering the thermal insulation of LPCS, we also proposed the concept of temperature difference weight ratio. As shown in Table 6, the temperature difference weight ratio actually increases with thickness of honeycomb core layer, so only with that in mind, 8 mm honeycomb core layer was the best choice for LPCS. But considering the capsule volume of stratospheric airships was usually too huge and the surface curvature of the buoyancy capsule was small, so local stress concentration of the airship envelope could easily lead to large transformation and cause the capsule to overpressure damage and blast quickly, and it will be necessary to try avoiding the thermal stress caused by the variation of temperature in the airship envelope. Therefore, the average irradiation of the airship in the stratosphere is considered as

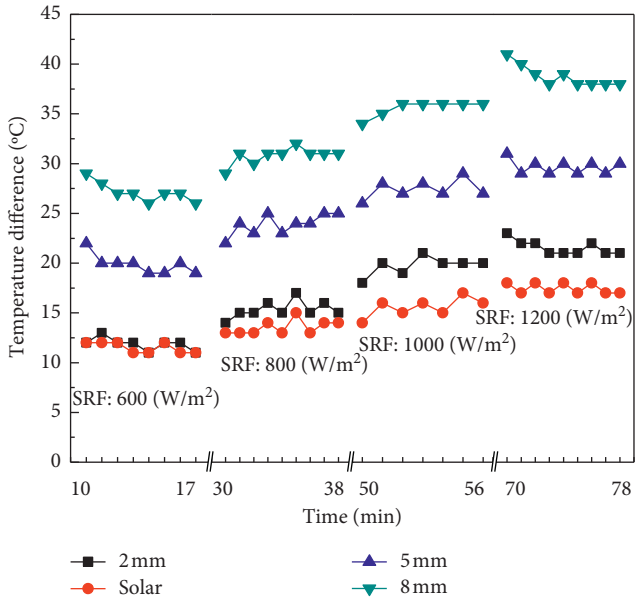

Figure 16: Thermal-barrier performance of the honeycomb core in different thickness.

Table 5: Deflection weight ratio with different thicknesses.

Thickness of honeycomb core layer (mm)	Increase of deflection (mm)	Increase of structure weight (g)	Deflection weight ratio (mm/(g/m^2))
2	5.6	6.1	0.0143
5	9.4	7.97	0.0184
8	4.5	9.4	0.0075

Table 6: Temperature difference weight ratio with different thicknesses.

Thickness of honeycomb core layer (mm)	Increase of temperature difference (°C)		Increase of structure weight (g)	Temperature difference weight ratio (°C/(g/m^2))
2	600 W/m^2	0.38	6.1	0.000973
	800 W/m^2	1.78		0.00456
	1000 W/m^2	4.14		0.0106
	1200 W/m2	4.11		0.0105
5	600 W/m^2	8.38	7.97	0.0164
	800 W/m^2	10.33		0.020
	1000 W/m^2	11.86		0.023
	1200 W/m^2	12.22		0.024
8	600 W/m^2	15.63	9.4	0.026
	800 W/m^2	17.22		0.029
	1000 W/m^2	20		0.033
	1200 W/m^2	21.33		0.035

1000 W/m^2, and the average temperature of the internal gas in the capsule is considered as −3.15°C (270 K) [28]. As shown in Figure 15, the lower surface temperature of the 5 mm honeycomb core layer of LPCS (−5.86°C or 267 K) is closer to the average temperature of the internal gas (−3.15°C or 270 K) than the 8 mm honeycomb core layer (−11.12°C or 262.03 K). According to Figure 12 and Table 5, the 5 mm honeycomb core layer shows the best flexibility of LPCS. In conclusion, in order to avoid the thermal stress caused by the variation of temperature in the airship envelope, the 5 mm honeycomb core layer is considered the optimal choice compared with 2 mm and 8 mm for LPCS.

8. Conclusion

This paper developed a lightweight photovoltaic composite structure (LPCS) according to the characteristics of the stratospheric airship capsule. In order to improve the flexible of the solar cell, we studied the mechanical properties in the different thicknesses of the honeycomb core for LPCS by FEM software and three-point bending test. The experiments were conducted to measure the temperature difference between upper and lower surfaces of the LPCS test samples under different solar radiation flux conditions. The experimental data were examined to evaluate the mechanical properties and thermal insulation performances of LPCS. Considering the quality of the whole structure, the paper finally gives the conclusion of the optimal thickness of the honeycomb core with more detailed descriptions.

(1) The LPCS in 5 mm have the best overall mechanical properties and the most appropriate thermal insulation performance, followed by 2 mm LPCS and 8 mm LPCS. Therefore, the 5 mm LPCS can be used as a suitable lightweight photovoltaic composite structure for application in the solar array on stratospheric airships.

(2) As the LPCS underwent high deformation during the bending test, simple linear beam theory was not sufficient to calculate the stress on the cells. A model similar to the one discussed in this paper was used to take into account the large deflections. By comparing with the experimental data, it is also possible to reduce the deviation by modifying specific parameters. The theory of the honeycomb core also requires further study.

(3) The different thicknesses of the honeycomb core layer for LPCS considering the structure weight have great influence on the mechanical properties and the thermal insulation performance. Therefore, it can be studied and applied to the optimized design of LPCS.

Nomenclature

$\alpha_{envelope}$: Absorptivity of envelope
α_{cells}: Absorptivity of solar cell array
T_{gas}: Temperature of the gas in the airship hull
β: Degree of flexing of the airship hull
ε: Strain of the material
P: Load on the solar cell
L: The span of three-point bending test
I: Inertia moment of the cell in flexion
B: Width of the cell
t: Thickness of the cell
θ: Deformed shape of the cell

δ: Deflection at the center
b: Depth of the honeycomb cell
l: Length of hole wall
E: Young's modulus
E_s: Elastic modulus of Nomex honeycomb paper
E_1: Elastic modulus in the x direction
E_2: Elastic modulus in the y direction
G: Shear modulus
G_1: Shear modulus in the x direction
G_s: Shear modulus of Nomex honeycomb paper.

Data Availability

The data used to support the findings of this study are available from the corresponding author upon request.

Conflicts of Interest

The authors declare that they have no conflicts of interest.

Acknowledgments

This work was supported by the National Natural Science Foundation of China under Grant Nos. 51775021 and 51307004, the Key Laboratory of Aircraft Advanced Design Technology (Beihang University), and the fifth youth top talent support program of Beihang University and Ministry of Industry

References

[1] L. Liao and I. Pasternak, "A review of airship structural research and development," *Progress in Aerospace Sciences*, vol. 45, no. 4-5, pp. 83–96, 2009.

[2] M. Lv, Z. Yao, L. Zhang, H. Du, J. Meng, and J. Li, "Effects of solar array on the thermal performance of stratospheric airship," *Applied Thermal Engineering*, vol. 124, pp. 22–33, 2017.

[3] K. Eguchi, Y. Yokomaku, M. Mori et al., "Feasibility study program on stratospheric platform airship technology in Japan," in *Proceedings of the 13th Lighter-Than-Air Systems Technology Conference*, Norfolk, VA, USA, July 1999.

[4] D.-M. Kim, Y.-G. Lee, W.-G. Kang, J.-W. Lee, and C.-H. Yeom, "Korea stratospheric airship program and current results," in *Proceedings of the 3rd Annual Aviation Technology, Integration, and Operations (ATIO) Forum (AIAA'03)*, pp. 2003–6782, Denver, CO, USA, November 2003.

[5] K. Harada, K. Eguchi, M. Sano, and S. Sasa, "Experimental study of thermal modeling for stratospheric platform airships," in *Proceedings of the AIAA's 3rd Annual Aviation Technology, Integration, and Operations (ATIO) Forum*, Denver, CO, USA, November 2003.

[6] W. Yao, X. Lu, C. Wang, and R. Ma, "A heat transient model for the thermal behavior prediction of stratospheric airships original," *Applied Thermal Engineering*, vol. 70, no. 1, pp. 380–387, 2014.

[7] H. Naito, K. Eguchi, and T. Hoshino, "Design and analysis of solar power system for SPF airship operations," in *Proceedings of the AIAA International Balloon Technology Conference*, Norfolk, VA, USA, June 1999.

[8] J. Li, M. Lv, D. Tan, W. Zhu, K. Sun, and Y. Zhang, "Output performance analyses of solar array on stratospheric airship with thermal effect," *Applied Thermal Engineering*, vol. 104, pp. 743–750, 2016.

[9] X. Li, X. Fang, and Q. Dai, "Research on thermal characteristics of photovoltaic array of stratospheric airship," *Journal of Aircraft*, vol. 48, no. 4, pp. 1380–1386, 2011.

[10] G. L. Eskind and R. Aanestad, "Multilayered flexible fire retardant isolative sheets comprising laminates of insulation layers and fire-retardant glass fiber layers and aluminum foil films," Google Patent 2001043972, 2001.

[11] A. Colozza, "Initial feasibility assessment of a high altitude long endurance airship," Tech. Rep. CR-21272, NASA, Washington, DC, USA, 2003.

[12] H. L. Yan, Q. Y. Zhang, L. Zhang et al., "Research progress of solar cell used in airship," *Journal of Materials Science and Engineering*, vol. 26, no. 5, pp. 824–828, 2008.

[13] A. Schoenmaker, "Certification and safety aspects relating to the transport of passengers on high altitude balloons in Europe," *Acta Astronautica*, vol. 100, pp. 1–10, 2014.

[14] J. Li, M. Lv, K. Sun, and W. Zhu, "Thermal insulation performance of lightweight substrate for solar array on stratospheric airships," *Applied Thermal Engineering*, vol. 107, pp. 1158–1165, 2016.

[15] P. Ren, Q. Meng, Y. Zhang, L. Zhao, X. Yuan, and X. Feng, "An unmanned airship thermal infrared remote sensing system for low-altitude and high spatial resolution monitoring of urban thermal environments: integration and an experiment," *Remote Sensing*, vol. 7, no. 10, pp. 14259–14275, 2015.

[16] Q. Dai and X. Fang, "Numerical study of forced convective heat transfer around airships," *Advances in Space Research*, vol. 57, no. 3, pp. 776–781, 2016.

[17] J. Xiong, J. B. Bai, and L. Chen, "Simplified analytical model for predicting the temperature of balloon on high-altitude," *International Journal of Thermal Sciences*, vol. 76, pp. 82–89, 2014.

[18] X. Li, X. Fang, Q. Dai, and Z. Zhou, "Modeling and analysis of floating performances of stratospheric semi-rigid airships," *Advances in Space Research*, vol. 50, no. 7, pp. 881–890, 2012.

[19] L. Zhang, L. J. Yao, J. S. Wang et al., "Exploring design of an ultra-light photovoltaic cell embedded structure," *Journal of Northwestern Polytechnical University*, vol. 30, no. 5, pp. 663–667, 2012.

[20] S. Schoenfelder, M. Ebert, C. Landesberger, K. Bock, and J. Bagdahn, "Investigations of the influence of dicing techniques on the strength properties of thin silicon," *Microelectronics Reliability*, vol. 47, no. 2-3, pp. 168–178, 2007.

[21] C. Qiu, Z. Guan, S. Jiang, and Z. Li, "A method of determining effective elastic properties of honeycomb cores based on equal strain energy," *Chinese Journal of Aeronautics*, vol. 30, no. 2, pp. 766–779, 2017.

[22] B. L. Lee, J. W. Song, and J. E. Ward, "Failure of spectra polyethylene fiber-reinforced composites under ballistic impact loading," *Journal of Composite Materials*, vol. 28, no. 13, pp. 1202–1226, 1994.

[23] P. Klemchuk, E. Myer, L. Gary, H. William, G. James, and A. Susan, "Investigation of the degradation and stabilization of EVA-based encapsulant in field-aged solar energy modules," *Polymer Degradation and Stability*, vol. 55, no. 3, pp. 347–365, 1997.

[24] S. Kunz-Douglass, P. W. R. Beaumont, and M. F. Ashby, "A model for the toughness of epoxy-rubber particulate

composites," *Journal of Materials Science*, vol. 15, no. 5, pp. 1109–1123, 1980.

[25] S. A. Hitchen and R. M. J. Kemp, "The effect of stacking-sequence on impact damage in a carbon fiber/epoxy composite," *Composites*, vol. 26, no. 3, pp. 207–214, 1995.

[26] J. Zhang and M. F. Ashby, "Buckling of honeycombs under in-plane biaxial stresses," *International Journal of Mechanical Sciences*, vol. 34, no. 6, pp. 491–509, 1992.

[27] K. Daryabeigi, "Heat transfer in high-temperature fibrous insulation," *Journal of Thermophysics and Heat Transfer*, vol. 17, no. 1, pp. 10–20, 2003.

[28] R. R. Meier, D. E. Anderson Jr., and M. Nicolet, "Radiation field in the troposphere and stratosphere from 240–1000 NM-I. General analysis," *Planetary and Space Science*, vol. 30, no. 9, pp. 923–933, 1982.